

# Efficient single image dehazing and denoising: An efficient multi-scale correlated wavelet approach



Xin Liu<sup>a,b,\*</sup>, He Zhang<sup>a,b</sup>, Yiu-ming Cheung<sup>c</sup>, Xinge You<sup>d</sup>, Yuan Yan Tang<sup>e</sup>

<sup>a</sup> College of Computer Science and Technology, Huaqiao University, Xiamen, 361021, China

<sup>b</sup> Xiamen Key Laboratory of Computer Vision and Pattern Recognition, Huaqiao University, Xiamen, 361021, China

<sup>c</sup> Department of Computer Science and Institute of Research and Continuing Education, Hong Kong Baptist University, Hong Kong SAR, China

<sup>d</sup> Department of Electronics and Information Engineering, Huazhong University of Science and Technology, Wuhan, 430074, China

<sup>e</sup> Department of Computer and Information Science, University of Macau, Macau SAR, China

## ARTICLE INFO

### Article history:

Received 27 September 2016

Revised 2 May 2017

Accepted 15 August 2017

Available online 23 August 2017

### Keywords:

Image dehazing

Multi-scale correlated wavelet

Open dark channel model

Soft-thresholding

## ABSTRACT

Images of outdoor scenes captured in bad weathers are often plagued by the limited visibility and poor contrast, and such degradations are spatially-varying. Differing from most previous dehazing approaches that remove the haze effect in spatial domain and often suffer from the noise problem, this paper presents an efficient multi-scale correlated wavelet approach to solve the image dehazing and denoising problem in the frequency domain. To this end, we have heuristically found a generic regularity in nature images that the haze is typically distributed in the low frequency spectrum of its multi-scale wavelet decomposition. Benefited from this separation, we first propose an open dark channel model (ODCM) to remove the haze effect in the low frequency part. Then, by considering the coefficient relationships between the low frequency and high frequency parts, we employ the soft-thresholding operation to reduce the noise and synchronously utilize the estimated transmission in ODCM to further enhance the texture details in the high frequency parts adaptively. Finally, the haze-free image can be well restored via the wavelet reconstruction of the recovered low frequency part and enhanced high frequency parts correlatively. The proposed approach aims not only to significantly increase the perceptual visibility, but also to preserve more texture details and reduce the noise effect as well. The extensive experiments have shown that the proposed approach yields comparative and even better performance in comparison with the state-of-the-art competing techniques.

© 2017 Elsevier Inc. All rights reserved.

## 1. Introduction

Haze is a common atmospheric phenomenon, where fog, dust, mist and other particles often deflect the light from its original course of propagation. Consequently, images captured in these unfavorable atmospheric conditions are often in a poor contrast and offer a limited visibility of the scene contents. In practice, haze is an annoyance problem to photographers since it degrades the image quality, and it is also a major threat to the reliability of many vision understanding applications, such as video surveillance, intelligent vehicles, satellite imaging, aerial imagery and target identification (Gibson et al., 2012) and so forth. For instance, the performance of feature detection will inevitably suffer from the low-

contrast scene in hazy images. Nevertheless, haze removal still remains a challenge problem due to the inherent ambiguity between the haze and the underlying scene. Furthermore, the captured images often contain some noise, which would be appeared and amplified during the dehazing process if it is ignored. Therefore, haze and noise removal are highly desirable in the degraded scenes, and improving the restoring performance will benefit many vision tasks practically.

In general, image dehazing can be considered as a process of removing haze effects in captured images and reconstructing the original colors of natural scenes. Intuitively, traditional scene contrast enhancement such as the histogram equalization (Zhu et al., 1999), linear mapping, retinex-mapping (Jobson et al., 1997) and the gamma correction (Katajamäki, 2003) are able to improve the perceptual quality of scene appearance. However, these methods do not consider the difference of haze thickness, which is proportional to object depths. Accordingly, these approaches often failed to compensate the haze degradation adaptively. To tackle this problem, some researchers selected to utilize some additional

\* Corresponding author at: College of Computer Science and Technology, Huaqiao University, Xiamen, 361021, China.

E-mail addresses: [xliu@hqu.edu.cn](mailto:xliu@hqu.edu.cn) (X. Liu), [hezhang91@gmail.com](mailto:hezhang91@gmail.com) (H. Zhang), [ymc@comp.hkbu.edu.hk](mailto:ymc@comp.hkbu.edu.hk) (Y.-m. Cheung), [youxg@hust.edu.cn](mailto:youxg@hust.edu.cn) (X. You), [yytang@umac.mo](mailto:yytang@umac.mo) (Y.Y. Tang).

information or multiple images to reduce the haze effect. For instance, [Narasimhan and Nayar \(2000\)](#) utilized some user-specified information interactively and exploited a physical model for haze removal. As the amount of light scattering was an unknown function of depth, such exploited model was often underconstrained if only one image was selected as a single input. Differently, [Schechner et al. \(2001\)](#) selected multiple images of same scene to remove the haze by different degrees of polarization. Although these two methods were able to improve the visibility of hazy images and produce impressive results, the interactive inputs specified by the users in the changing scenes may not be easily obtained while the multiple images were not available in practice.

In recent years, significant progresses in single image haze removal have been made by using reasonable priors or assumptions. Along this way, [Tan \(2008\)](#) aimed to maximize the local contrast to restore the degraded scenes, provided that the images with enhanced visibility have more contrast than images plagued by bad weather. Although this method is able to improve the visibility of hazy images and produce impressive results, it often tends to be over-saturated and may fail to maintain the color fidelity because the haze-free images do not always have the maximum contrast. Similarly, [Fattal \(2008\)](#) estimated the transmission through a refined image formation model, in which the cost functions of surface shading and transmission were considered to be statistically uncorrelated. [Kratz and Nishino \(2009\)](#) assumed that the scene albedo and depth were two statistically independent latent layers, and thus modeled the image with a factorial Markov random field (FMRF) for haze removal. These two approaches were able to produce visually impressive results, but which may fail to remove the haze effects where these assumptions are broken. For instance, these two methods required the surface shading and transmission to vary significantly in a local patch, which were not reliable in dense hazy regions.

Until recently, [He et al. \(2009, 2011\)](#) leveraged an empirical observation that the local patches in haze-free images often contained some low albedo values in at least one color channel. Inspired by this finding, they proposed a dark channel prior (DCP) to estimate the haze thickness and utilized the soft-mating technique to reduce the haze effect. By using DCP information, some improved works ([Gibson and Nguyen, 2013](#); [He et al., 2013](#); [Tarel and Hautiere, 2009](#); [Xie et al., 2010](#)) were also developed to estimate the haze thickness and attempted to recover a high-quality haze-free image. Despite these remarkable progresses have been exploited and the satisfactory performances in terms of better visibility are obtained, the DCP may be invalid when the scene appearance is inherently similar to the airlight or the input hazy image contains some significant noises. Later, [Meng et al. \(2013\)](#) introduced a boundary constraint on the transmission function, while [Fattal \(2014\)](#) presented a novel color-line pixel regularity to obtain a more reliable transmission. However, if the scene is very bright, the transmissions estimated by these two methods may be severely underestimated across the entire image. Later, [Zhu et al. \(2015\)](#) created a linear model to estimate the scene depth under a novel color attenuation prior and learned the model parameters in HSV space. Although this approach can produce visually pleasing performance, it often fails to remove the dense haze in the remote scenes.

Evidently, most of the existing image dehazing approaches selected to remove the haze effect in spatial domain. Differently, [Du et al. \(2002\)](#) first decomposed the high-resolution satellite images into different spatial layers, and then utilized the frequency characteristics to achieve haze removal. Nevertheless, the primary drawback of this approach in its present form is to select the decomposition level and collect a haze-free reference image precisely. In addition, this approach did not consider the coefficient relationships of different spatial layers, and it is unsuitable for

haze removal in natural images. Later, [Rong and Jun \(2014\)](#) applied the wavelet transform to achieve image dehazing, in which the unsharp masking algorithm was applied to improve the image contrast while the dual-threshold algorithm was adopted to enhance the clarity of details. However, this approach often induced a blur reconstruction and the visual performance was a bit poor. The main reason lies that the straightforward enhancement with nonlinear compensation would change the coefficient relationships such that the wavelet reconstruction may fail to preserve the original texture details. Despite these remarkable progresses have been exploited for haze removal, the aforementioned approaches may be invalid when the input hazy image contains significant noises.

In this paper, we present a novel perspective for single image dehazing using multi-scale correlated wavelet framework. As opposed to most recent popular approaches that removing the haze effect in spatial domain, our work treats the dehazing problem in frequency domain and is inherently different from the works ([Du et al., 2002](#); [Rong and Jun, 2014](#)). The method in [Du et al. \(2002\)](#) highly relies on another haze-free reference image of the same scene, while the approach in [Rong and Jun \(2014\)](#) did not consider the scene depth physically. By contrast, our proposed approach derives the haze under physical model and could remove haze effect in a single input, which improves the state-of-the-art methods by providing the following three contributions: 1) Taking advantage of haze typically distributes in the low frequency spectrum, we propose an open dark channel model to reduce the haze effect in this part efficiently; 2) Our dehazing framework is the first to exploit the relationships of wavelet coefficients for haze removal and texture enhancement simultaneously; 3) The proposed approach aims not only to significantly increase the perceptual visibility of haze scene, but also to reduce the noise effect as well. The experiments have shown its outstanding performance.

The rest of the paper is structured as follows: [Section 2](#) introduces the popular atmospheric scattering model, haze observations in frequency domain and wavelet analysis model. In [Section 3](#), we present the proposed framework and its implementation details. [Section 4](#) provides the experimental results and discussions. Finally, we draw a conclusion in [Section 5](#).

## 2. Background and observation

This section shall first overview the atmospheric scattering model, and subsequently elaborate the motivation of haze removal in frequency domain. Finally, the core idea of multi-scale wavelet decomposition is simplified for easy readable.

### 2.1. Atmospheric scattering model

In computer vision, the formation of hazy images is usually described by the atmospheric scattering model ([Narasimhan and Nayar, 2003](#)):

$$I(x) = J(x)t(x) + A(1 - t(x)), \quad (1)$$

where  $I$  is an observed hazy image,  $J$  is the scene radiance to be recovered,  $x=(x, y)$  indexes the pixel position,  $A$  is the global atmospheric light, and  $0 \leq t(x) \leq 1$  is the medium transmission describing the portion of the light that is not scattered and reaches to the camera. In a homogeneous atmosphere, the transmission  $t$  can be further expressed as  $t(x) = e^{-\beta d(x)}$ , where  $d(x)$  is the distance from the scene point to the camera, and  $\beta$  is the scattering coefficient of the atmosphere. In the right-hand side of Eq. (1), the first term perceived as direct attenuation often decreases the brightness, while the second term known as airlight could compensate the brightness and decrease the saturation.

The goal of image dehazing is to recover the scene radiance  $J(x)$  from  $I(x)$  based on Eq. (1). This requires us to estimate the transmission function  $t(x)$  and the global atmospheric light  $A$ . Once  $A$

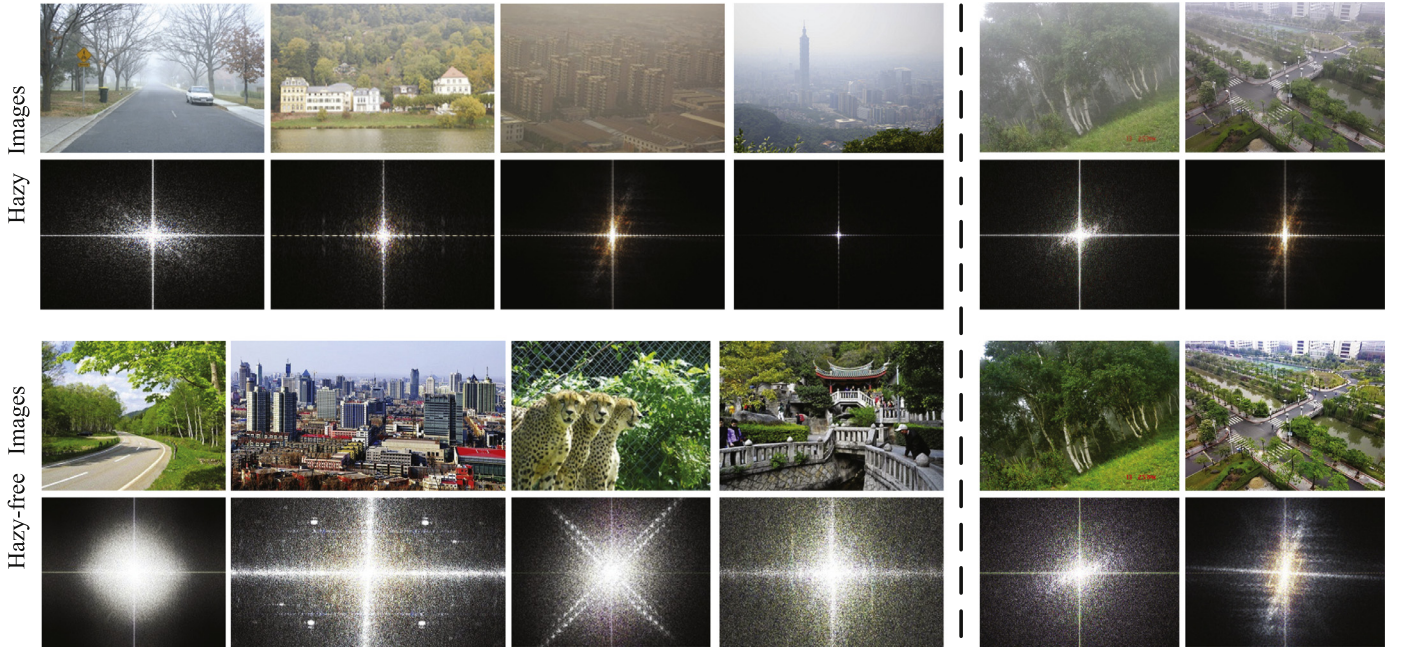


**Fig. 1.** The Fourier transform applied to hazy and haze-free images, respectively. The top examples are the input hazy images and below examples are the haze-free images, in which the right parts are the haze and haze-free image pairs.

and  $t$  are known, the  $J$  can be well recovered by inverting the atmospheric scattering model:

$$J(x) = (I(x) - A)/\max(t(x), \sigma) + A. \quad (2)$$

where  $\sigma$  is a lower bound utilized to restrict the transmission, and a typical value can be set at 0.1 (He et al., 2011).

### 2.2. Observations of haze analysis in frequency domain

In general, the direct attenuation is often characterized by fast spatial variation due to the surface reflectance and light changing, while the airlight is modeled by slow spatial variation corresponds to the atmospheric scattering. Since the haze is mainly generated by atmospheric scattering and widely spread, the spatial variation of its distribution will be very slow and smooth. Referring to the image processing in the frequency domain, it is reasonable to assume that the haze almost resides in the low frequency components.

Representative observations are shown in Fig. 1, it can be clearly found that the haze-free images often exhibit more high frequency spectrum, while the hazy images always deliver more low frequency spectrum. The similar observations are also appeared within the haze and haze-free image pairs. That is, the haze distribution typically resides within the spatially lower frequency components. Therefore, it is quite natural to remove the haze in the low frequency part practically.

### 2.3. Multi-scale wavelet analysis model

In recent years, wavelets have recently emerged as an effective tool to analyze image information (Mallat, 1989), because they provide a natural partition of the image spectrum into multi-scale and oriented sub-bands. A wavelet basis for multi-scale analysis is comprised of a hierarchy of linear spaces  $\{V^{j+1} | V^{j+1} \subset V^j\}$  and its orthogonal complement space  $\{W^{j+1} = V^j/V^{j+1}\}$ . Accordingly, a wavelet basis can be constructed by following two functions: the scaling function  $\phi$  and the wavelet function  $\psi$ .

$$\phi(x) = \sqrt{2} \sum_k l(k) \phi(2^j x - k), \quad (3)$$

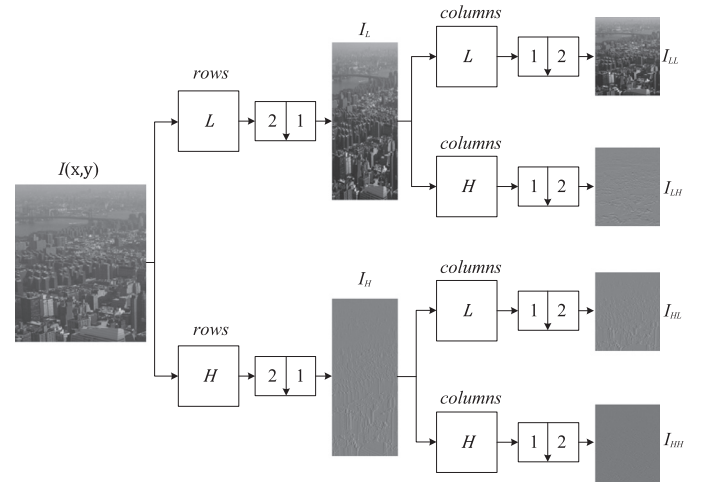


**Fig. 2.** One stage of 2-D multi-scale wavelet decomposition.

$$\psi(x) = \sqrt{2} \sum_k h(k) \psi(2^j x - k). \quad (4)$$

where  $l(k)$  represents the lowpass coefficient and it must satisfy the condition  $\sum_k l(k) = \sqrt{2}$ ,  $h(k)$  denotes the highpass coefficient and it is required to be orthogonal to the lowpass coefficient, i.e.,  $h(k) = (-1)^k l(1-k)$ . Specifically,  $\sqrt{2}$  maintains the norm of the scaling function with the scale of two.

As shown in Fig. 2, the 1-D multi-resolution wavelet decomposition can be easily extended to two dimensions by introducing separable 2-D scaling and wavelet functions as the tensor products of their 1-D complements:

$$\begin{cases} \phi_{LL}(x, y) = \phi(x)\phi(y), & \psi_{LH}(x, y) = \phi(x)\psi(y) \\ \psi_{HL}(x, y) = \psi(x)\phi(y), & \psi_{HH}(x, y) = \psi(x)\psi(y) \end{cases} \quad (5)$$

For image analysis, the 2-D wavelet analysis operation equivalently consists of filtering and down sampling horizontally using the 1-D low pass filter  $L$  and high pass filter  $H$  to each row in the

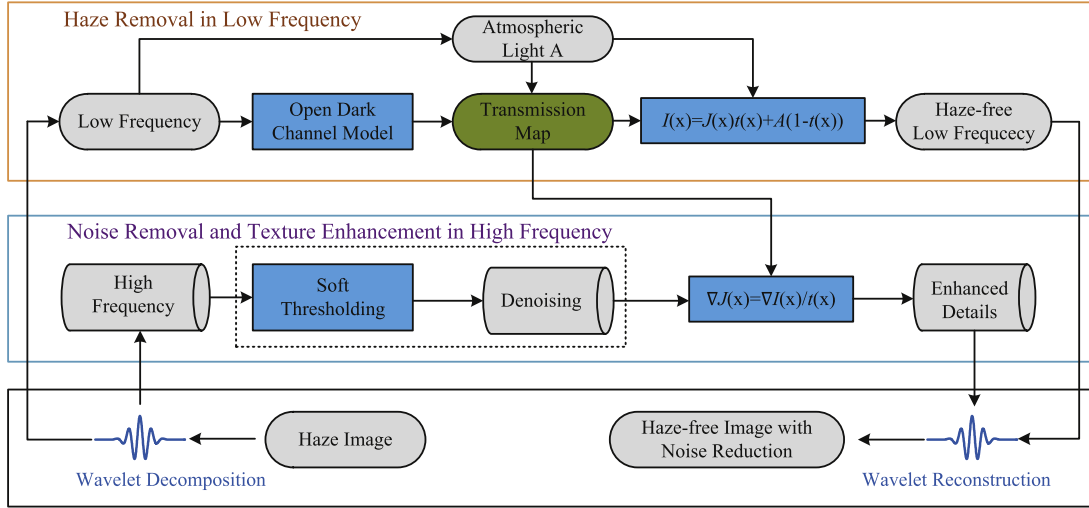


Fig. 3. The flowchart of the proposed image dehazing and denoising framework.

image  $I$  (obtain  $I_L$  and  $I_H$ ) and followed by vertically filtering and down sampling using  $L$  and  $H$  to each column. As a result, four sub-images  $I_{LL}(x, y)$ ,  $I_{LH}(x, y)$ ,  $I_{HL}(x, y)$  and  $I_{HH}(x, y)$  of one level of decomposition can be obtained. Specifically,  $I_{LL}(x, y)$  is a smooth sub-image corresponding to the low-frequency band (i.e., subsampled version of the original image), while  $I_{LH}(x, y)$ ,  $I_{HL}(x, y)$  and  $I_{HH}(x, y)$  denote the high-frequency bands with respected to the horizontal, vertical and diagonal details of the original image, respectively.

### 3. The proposed methodology

As discussed in Section 2.2, it is natural to focus on haze removal in the low frequency band and at the same time enhance the texture details in the high frequency bands. In addition, the significant noise is almost resided in the high frequency spectrum, which motivates us to reduce the noise impacts in this part extensively. Benefits from wavelet decomposition, as shown in Fig. 3, we propose an open dark channel model (ODCM) to remove the haze effect in low frequency part. Then, we select to reduce the noise impact and utilize the estimated transmission value in ODCM to further enhance the texture details in high frequency parts adaptively. Finally, the haze-free image can be well restored via the wavelet reconstruction.

#### 3.1. Haze removal in low frequency

Since the haze typically distributes with spatially lower frequency band, the popular atmospheric scattering model can be well applied to remove the haze effect from this part extensively. Suppose the intensity value of sub-image  $I$  with respected to the lower frequency band is normalized between 0 and 1, the corresponding scene radiance  $J$  is always bounded and we can derive the following constraint for  $J$ :

$$0 \leq J^c(x) \leq 1, \forall c \in \{r, g, b\}, \quad (6)$$

where  $c$  denotes the color channel in RGB space, 0 and 1 are the physical bounds to avoid undershoot and overshoot of resulting image. By examining the physical properties in Eq. (1), it is easy to obtain  $t(x) = \|I(x) - A\| / \|J(x) - A\|$ , and the above requirement on  $J(x)$ , in turn, imposes a boundary constraint on  $t(x)$ . Suppose that the global atmospheric light  $A$  is given, we can derive the following constraint on  $t(x)$ :

$$0 \leq t_b(x) \leq t(x) \leq 1, \quad (7)$$

where  $t_b(x)$  is the lower bound of  $t(x)$ , given by

$$t_b(x) = \min \left\{ 1 - \min_c \left\{ \frac{I^c(x)}{A^c}, \frac{\tilde{I}^c(x)}{\tilde{A}^c} \right\}, 1 \right\}, \quad (8)$$

where  $\tilde{I}^c = 1 - I^c$  is the inverse image of  $I^c$  and  $\tilde{A}^c = 1 - A^c$ . Evidently, Eq. (7) shows the large ambiguity in identifying the correct  $t$ . Alternatively, estimating optimal transmission  $t$  can be converted into the following energy minimization problem:

$$\arg \min_t \Phi(J(x)), \quad \text{s.t.} \begin{cases} t_b(x) \leq t(x) \leq 1, \\ J(x) = (I(x) - A)/t(x) + A \end{cases} \quad (9)$$

where  $\Phi(\cdot)$  is an energy function that prompts the recovered image  $J$  to meet the natural image statistics (e.g., DCP) and penalizes the solution of  $t$  far away from the natural image statistics (e.g., total variation (Chen et al., 2016)). That is, the optimal solution of  $t$  should be piecewise smooth and contain less statistical information about scene appearance. However, on the one hand, it is extremely difficult to find a good form of  $\Phi(\cdot)$  in the area of image restoration. On the other hand, the regularization term on transmission  $t$  can be fairly complicated when a particular form of  $\Phi$  is employed. Instead of designing a particular form of  $\Phi$ , He et al. (2011) first assume that the transmission  $t$  is locally constant, and then apply a minimum filter to achieve a tight lower bound of  $t$ :  $\tilde{t}(x) = 1 - \min_{y \in \Omega_x} \left( \min_c \left\{ \frac{I^c(y)}{A^c} \right\} \right)$ , where  $\Omega_x$  is a local patch centered at  $x$ . Nevertheless, this method without inherent boundary constraint often tends to over-estimate the thickness of the haze, which cannot handle the very bright regions, e.g., sky part. In most cases, the optimal global atmospheric light  $A$  is a little darker than the brightest pixels in the image. Under such circumstance, the DCP often fails to adapt those brightest pixels. Therefore, the boundary constraint regularized on scene transmission is necessary. In addition, it can be further found that the minimum operator may result in an inconsistent profile with the input image. To tackle these issues, we add the inherent boundary constraint and take a morphological open operation to precisely estimate the transmission map:

$$\tilde{t}(x) = 1 - \text{open}_B \left( \min_c \left\{ \frac{I^c(y)}{A^c}, \frac{\tilde{I}^c(y)}{\tilde{A}^c} \right\} \right). \quad (10)$$

$$\text{open}_B(I) = \max_B \{ \min \{ I(x-s, y-t) - B(s, t) \} + B(s, t) \} \quad (11)$$

where  $B(s, t)$  is the structuring element and its size is  $s \times t$ . In particular, the square structuring element is employed and its corre-

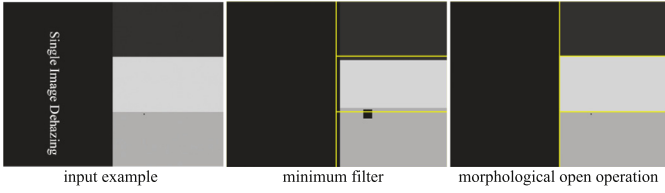


**Fig. 4.** A synthetic image processed by minimum filter and the morphological open operation, in which the size of synthetic image is  $400 \times 300$  and the size of local patch  $\Omega$  is  $20 \times 20$ .

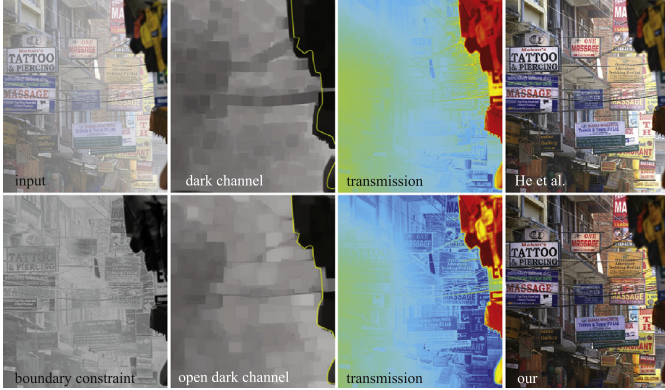


**Fig. 5.** Image dehazing results obtained by DCP and ODCM, in which the image size is  $332 \times 500$  and the size of local patch  $\Omega$  is  $20 \times 20$ . From left to right of the top row: original hazy image, dark channel image, refined transmission map and the dehazing result obtained by He et al. (2011); From left to right of the bottom row: boundary map constrained by  $\min \left\{ \frac{F(y)}{A_c}, \frac{F(y)}{A_c} \right\}$ , open dark channel image, refined transmission map and the dehazing result obtained by our proposed approach.

sponding size is generally set as the same to the local patch  $\Omega_x$ . Intrinsically, the open operation is able to remove small bright details and impose spatial coherency. Therefore, such operation would be more reasonable to outline a precise scene transmission. Typical examples are shown in Figs. 4 and 5, in which the yellow curve labels the profile of the different views. In Fig. 4, the edges of the synthetic image are changed within the result processed by minimum filter, but which can be well preserved by open operation. In Fig. 5, the minimum filter has dilated the objects nearby, and the thickness of haze around the dark wire was underestimated. In contrast to this, the hazy layer estimated by the proposed boundary constraint and morphological open filter has a more consistent profile with the input image and the edges of estimated transmission map are well preserved. As a result, the haze is well removed between the neighbouring regions of different views (i.e., distant view and close view). For simplicity, this improved transmission estimation method is called open dark channel model (ODCM).

As stated in Section 2.1,  $t(x)$  is generally a piecewise smooth function and it is imperative to smooth  $t$  by an edge preserving filter. In the past, guided filter (He et al., 2013), derived under the assumption of linear relation between the filtered image and the guide image, can be effectively utilized for preserving the edges. However, such filter often limits its power in smoothness. To ensure this constraint, the domain transform filter (Gastal and Oliveira, 2011), embedded with edge-aware kernels and favored for its fast implementation, is further applied for transmission smoothing.

By examining the Eqs. (1) and (10), it is imperative to search an appropriate atmospheric light  $A$  for evaluating transmission  $t$  and achieving haze removal. As suggested in work (He et al., 2011), the brightest pixel value in the 0.1% pixels with the largest dark

channel values is taken as atmospheric light  $A$ . However, this selection only considers a single pixel, and it may be affected by apparent noise. In the low frequency part, we select to pick the top 0.1 percent brightest pixels in the open dark channel values and take the mean of these values as the global atmospheric light  $A$ , featuring on robustness to the noise. With well estimated global atmospheric light  $A$  and transmission function  $t$ , the scene radiance  $J$  can be well recovered by Eq. (2).

### 3.2. Noise removal and texture detail enhancement

Remarkably, most of the current dehazing approaches often suffer from the significant noise and cannot remove them synchronously. Fortunately, our proposed approach selects to decompose the hazy image into low and high frequency parts, whereby the noise (e.g., Gaussian noise) is almost left in the high frequency parts. Benefit much from this separation, such noise can be effectively removed by adding soft-thresholding operation  $\mathcal{S}_\tau$  at the high frequency parts directly (Donoho, 1995):

$$\mathcal{S}_\tau(x) = \text{sign}(x) \cdot (|x| - \tau) \quad (12)$$

where  $\tau$  is the threshold value and it is usually estimated by the median of the first level decompositions.

Since the low-frequency band and high-frequency bands are correlatively obtained by wavelet decomposition, the coefficients of different parts are closely related. Under such circumstances, if we perform a wavelet reconstruction by selecting the recovered low-frequency part and unchanged high-frequency parts, the recovered performance would be quite unnatural due to the disturbed coefficient relationships. To resist this attack, it is reasonable to correlate the coefficients of low-frequency part and high-frequency parts adaptively. To this end, we heuristically utilize the estimated transmission value in ODCM to maintain the coefficient relationships and simultaneously enhance the texture details in the high frequency parts efficiently.

Given the image degradation equation  $I(x) = J(x)t(x) + A(1 - t(x))$ , it is imperative to find the reasons for the texture degradation. In computer vision community, image textures generally characterize the details of the object appearance, which can be visually described by various oriented gradients within the image. That is, the oriented gradient cues contain many texture features, and such gradients can be further considered as the sources of high frequency components in frequency domain. Since  $A$  is the global atmospheric light, by taking the gradients of Eq. (1), the following equations are obtained:

$$\begin{aligned} \nabla I(x) &= \nabla(J(x)t(x)) + \nabla(A(1 - t(x))) \\ &= \nabla J(x) \cdot t(x) + \nabla t(x) \cdot (J(x) - A)t \end{aligned} \quad (13)$$

As indicated in work (Fattal, 2014), it is to be noted that the transmission  $t(x)$  is a piecewise smooth function, and its value in most image patches does not vary from its average by more than 0.5%. Therefore, the transmission  $t(x)$  can be generally considered as a local constant in a very small patch, and the value of its gradient is almost close to zero. Accordingly, Eq. (13) can be further relaxed to its equivalent form:

$$\nabla I_\Omega(x) = t_\Omega \cdot \nabla J_\Omega(x) \quad (14)$$

where  $\Omega$  is a local path with small size. Since transmission  $t$  is in the range  $[0, 1]$ , thus  $\nabla I$  has a smaller magnitude than  $\nabla J$ . As a result, the visibility is reduced and the object textures are degraded. Note that, Eq. (14) implies that the high frequency parts of hazy image are degraded due to the multiplication  $t$ . Benefit much from wavelet decomposition, the high frequency elements, i.e., horizontal, vertical and diagonal details can be also regarded as horizontal,

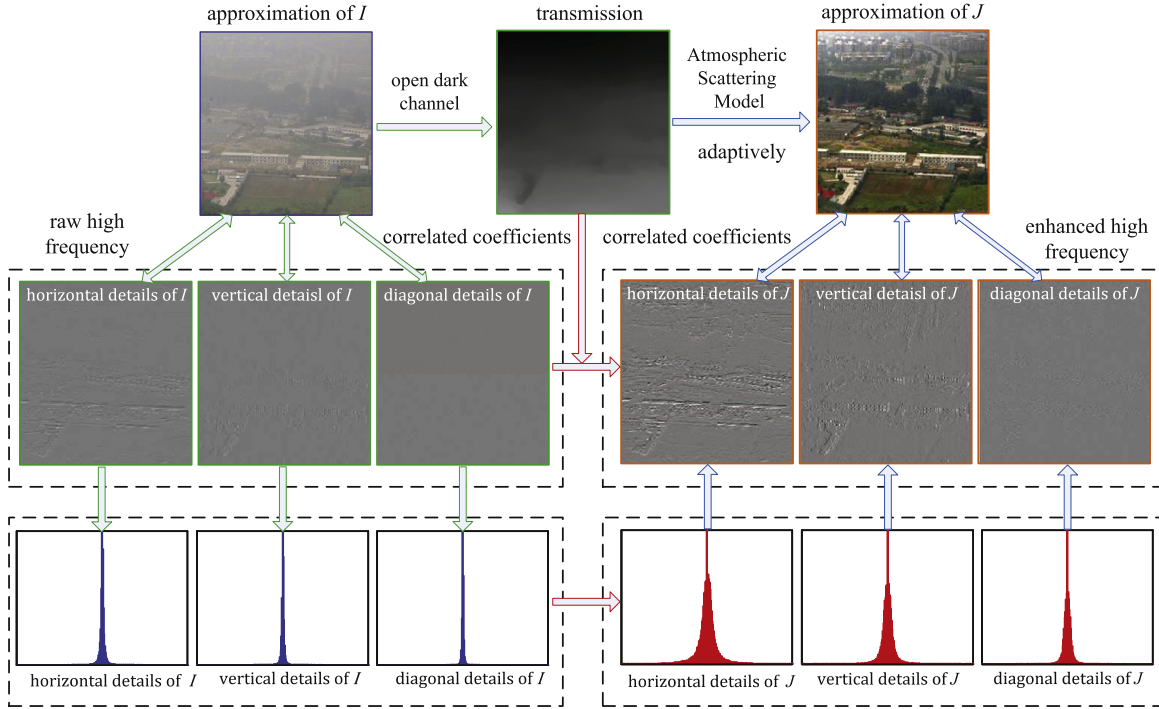


Fig. 6. The multi-scale correlated wavelet coefficients for adaptive high frequency texture enhancements.

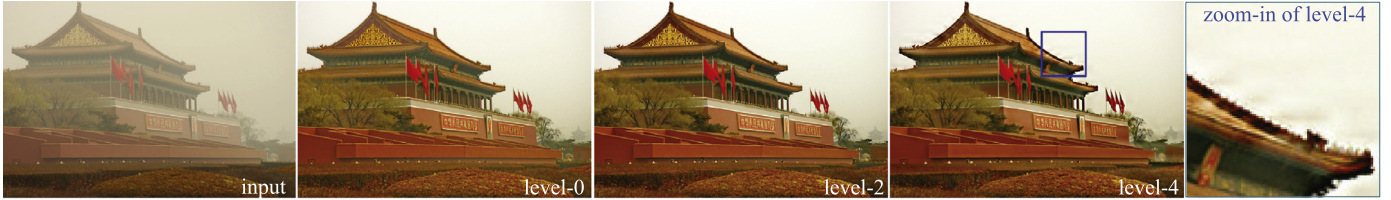


Fig. 7. The image dehazing performances obtained by different decomposition levels, in which level-0 means no decomposition.

vertical and diagonal gradients. Referring to Eq. (14), it can be easily inferred:

$$\nabla I_{\Omega} = \{\partial_x I_{\Omega}, \partial_y I_{\Omega}, \partial_y \partial_x I_{\Omega}\} = t_{\Omega} \cdot \{\partial_x J_{\Omega}, \partial_y J_{\Omega}, \partial_y \partial_x J_{\Omega}\} \quad (15)$$

$$\begin{cases} \partial_x I_{\Omega} = t_{\Omega} \cdot \partial_x J_{\Omega} & \text{horizontal} \\ \partial_y I_{\Omega} = t_{\Omega} \cdot \partial_y J_{\Omega} & \text{vertical} \\ \partial_y \partial_x I_{\Omega} = t_{\Omega} \cdot \partial_y \partial_x J_{\Omega} & \text{diagonal.} \end{cases} \quad (16)$$

This local linear model enables us to enhance the texture details of the high frequency, provided that the transmission  $t$  of the input image is obtained in advance. Fortunately, the transmission  $t$  can be well estimated through the low frequency components. With the above gradients, we can correlate the wavelet coefficients between the recovered low frequency part and high frequency part adaptively. Typical example is shown in Fig. 6, it can be found that the texture details are enhanced apparently within the high frequency parts. More importantly, the coefficient relationships between the high frequency parts and the recovered low frequency part almost remain unchanged, thereby the recovered scenes would be natural and clear enough.

In a theoretical way, the more level we split, the more details we can manipulate to achieve the better results. Evidently, the more decomposition would lead to multiple transmission estimation, which is time-consuming. For computationally tractable and transmission smoothness, we employ the bilinear interpolation technique to obtain transmission at the previous decomposition. The dehazing results obtained by different decompositions are shown Fig. 7, it can be observed that the two level decomposition has achieved a similar result as the three level decomposition, and

the recovered sky region is more nature than the results with no decomposition. Remarkably, the transmission estimated by upsampling technique is not accurate enough with the texture edges. As a result, the more level we split, the less information is left in low frequency part. Consequently, the transmission may not be accurately estimated for efficient haze removal. To balance the trade-off between the decomposition level and dehazing performance, the decomposition level is generally set at 2 in all the experiments.

### 3.3. Wavelet reconstruction

After the haze removal in low frequency part, noise removal and texture detail enhancement in the high frequency parts, the haze-free image can be directly obtained by the wavelet reconstruction. Since the scene radiance is usually not as bright as the atmospheric light, the image after haze removal often looks a bit dim. To tackle this problem, we refer to the works (Berman et al., 2016; He et al., 2013) and also increase the exposure of  $J$  for better visual quality.

## 4. Experimental results

In the experiments, the public available natural hazy images<sup>1</sup> were selected for testing, and the fast wavelet transform (Rioul and Duhamel, 1992) with “sym4” filter was chosen to decompose the image. Meanwhile, the patch size was fixed at

<sup>1</sup> From [http://www.cs.huji.ac.il/~raananf/projects/dehaze\\_cl/](http://www.cs.huji.ac.il/~raananf/projects/dehaze_cl/).

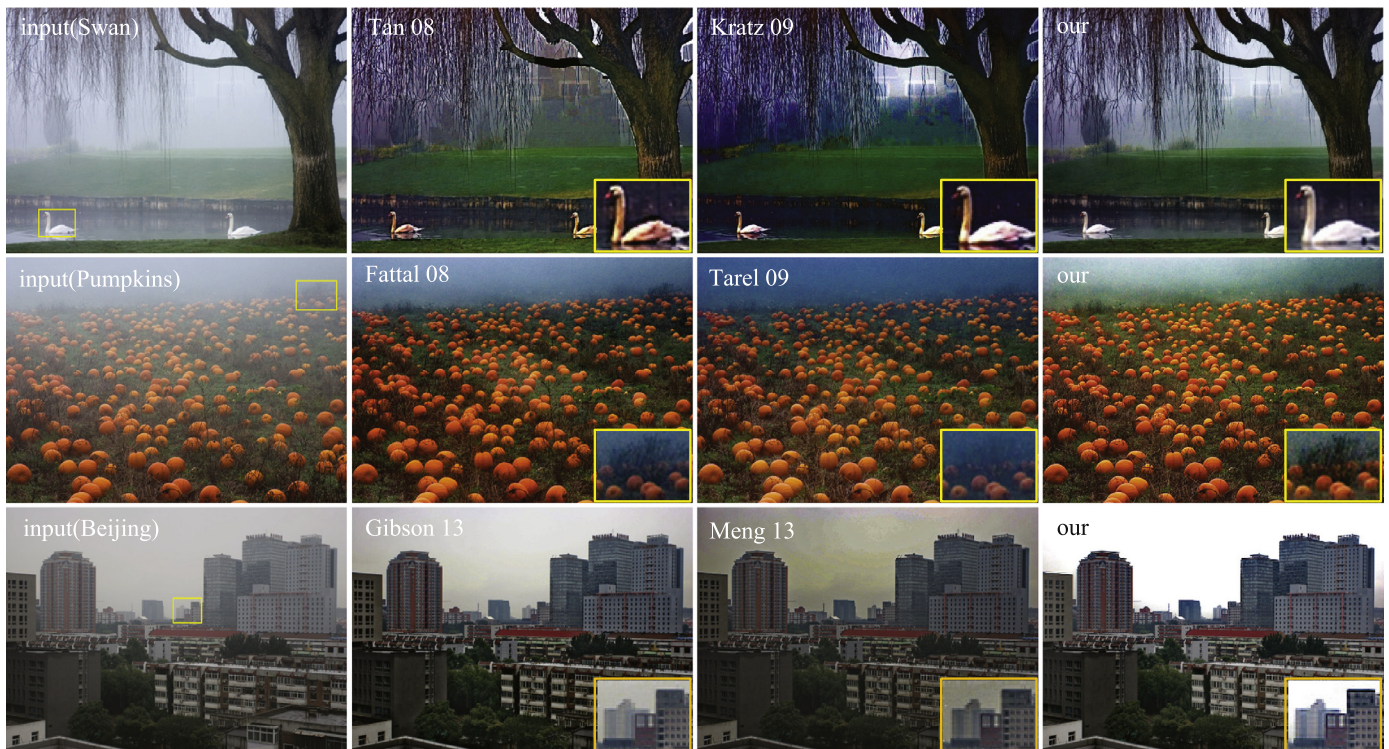


Fig. 8. Representative image dehazing results (i.e., Swans, Pumpkins and Beijing images) obtained by different approaches.

$8 \times 8$  in all the testing examples. To evaluate the dehazing performance, nine competing approaches, simply denoted as Tan (2008), Fattal (2008), Kratz and Nishino (2009), Tarel and Hautiere (2009), Gibson and Nguyen (2013), He et al. (2011), Meng et al. (2013), Zhu et al. (2015), and Berman et al. (2016) were selected for comparison. Meanwhile, we chose the other suggested parameters as the authors have given in all the experiments.

#### 4.1. Dehazing performance

Typical dehazing performances were shown in Figs. 8 and 9, respectively. Although the visibility maximizing scheme in Tan (2008) was able to augment the image contrast and greatly improve the scene visibility, the color appearance within the recovered scenes were often over saturated (e.g., swans), and some halo artifacts usually appeared around the recovered edges. The main reason lies that the visibility is maximized only when the intensities of some pixels are below zero, and this assumption is not physically valid in practice. By exploiting the priors of natural images and depth statistics, Kratz and Nishino (2009) adopted a factorial MRF to model a foggy image and the aesthetically pleasing results can be obtained. However, this method often tended to underestimate the transmission and thus induced some halo artifacts (e.g., trees). Fattal (2008) selected to estimate the transmission by using sufficient color information and variance, through which the haze effect can be significantly reduced. Unfortunately, if the haze is very dense, the color information will be very faint and therefore the transmission would be wrongly estimated for scene enhancement. Tarel and Hautiere (2009) and Gibson and Nguyen (2013) estimated the atmospheric veil by respectively applying a fast median filter and an adaptive wiener filter to the minimum components of an observed image, which incorporate an advantage of linear complexity. Nevertheless, the dehazing results obtained by these two approaches were not quite visually compelling, and some details are lost in the dark region due to the unremoved haze. Similarly, Meng et al. (2013) also has resulted in a bit poor

dehazing performance due to the inaccurate transmission estimation along the texture edges.

The recent image dehazing works, He et al. (2011), Zhu et al. (2015) and Berman et al. (2016) were popularly known for their robustness. After in-depth study of these approaches, we found that the patch-based DCP approach (He et al., 2011) often dilated the nearer objects and produced unpleasing results. Meanwhile, the matting Laplacian or guide filter utilized to regularize the transmission was known to achieve less smoothing and often transferred some texture details into the transmission map. Accordingly, this type of approach has induced an overall reduction of contrast at the distant regions, (e.g., Mountain and Hillside). To remove the haze, Zhu et al. (2015) created a linear model and utilized the color attenuation prior to model the scene depth. However, there still existed a small proportion of haze in the corresponding dehazing results (e.g., Mountain). The main reason can be attributed to the difficult parameter learning from training example pairs. Note that, Berman et al. (2016) has produced quite visually compelling results, but which may also result in a bit poor performance at some local regions (e.g., houses in the Florence image and island in the Manhattan). By contrast, our proposed approach almost yielded very comparative and even better results than these competing techniques. It is to be noted that the proposed approach not only has significantly improved the visibility of the distant views, but also has enhanced the texture details and simultaneously maintained the original color appearances. In addition, the halo artifacts within our recovered results were quite small.

#### 4.2. Quantitative comparison

In the past, most of existing dehazing algorithms often select to subjectively evaluate the dehazing performance based on human visual system, because objective quality assessment is a very challenging problem since a perfect quality dehazed image is not available as a reference. In general, haze often reduces the visible

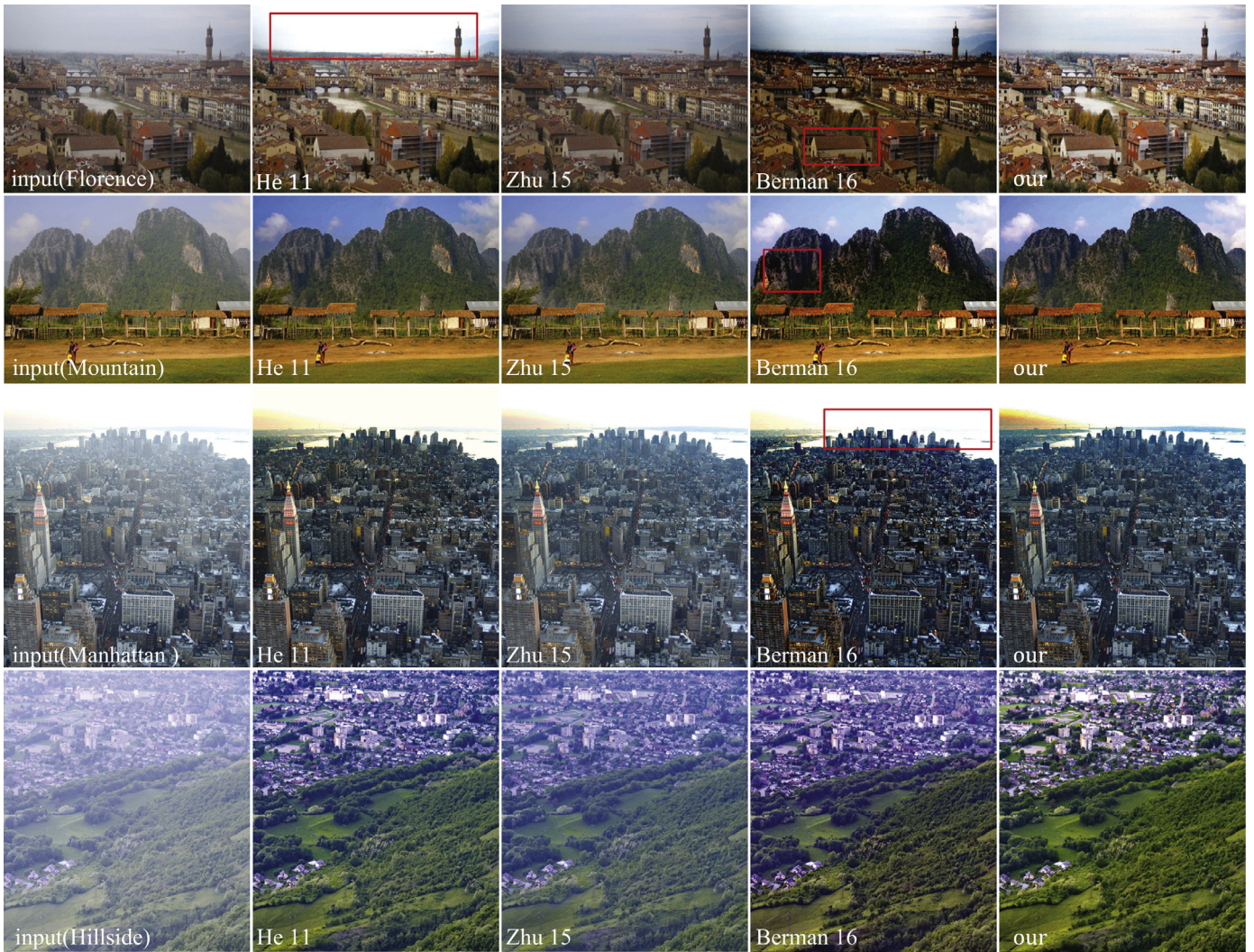


Fig. 9. Representative image dehazing results (i.e., Florence, Mountain, Manhattan and Hillside images) obtained by different approaches.

edges and texture information in the scene. Therefore, the restoration can be heuristically measured by the numbers of visible edges and texture details. Similar to the work (Tarel and Hautiere, 2009), three well-known quantitative metrics, visible edge ratio  $e$ , gradient ratio  $\bar{r}$  and saturated pixel ratio  $\sigma$ , are selected for evaluating the dehazing performance (Ancuti and Ancuti, 2013; Hautiere et al., 2008; Xu et al., 2014). The interested readers may refer to the work (Hautiere et al., 2008) for their mathematical definitions. Physically, the first metric indicates that the edges are not visible in the original image but appear in the restored image, the middle metric measures the degree of average visibility enhancement, and the last metric provides the percentage of pixels which become completely black or completely white after restoration. In practice, the higher  $e$  and  $\bar{r}$  often indicate more texture details and thus produce a better restoration result, while the smaller  $\sigma$  represents the less information loss.

In particular, we referred to works (Berman et al., 2016; He et al., 2013) and increased the exposure for all the restored examples. Accordingly, the quantitative values obtained by three very competing works (Berman et al., 2016; He et al., 2011; Zhu et al., 2015) and our method were shown in Table 1. It can be found that the performances obtained by He et al. (2011) and Berman et al. (2016) have resulted some negative  $e$  values. That is, some visible edges obtained by these two methods were lost in

the restored performances (e.g., marked by red rectangles in the Florence and Manhattan). Although Berman et al. (2016) has generated a bit larger  $\bar{r}$  values in Swan and Manhattan images, the color appearances of these two examples were a bit over saturated, e.g., some pixels were truncated to black or white. Similarly, Zhu et al. (2015) has almost yielded the lowest  $\sigma$  values, but its performance has resulted in a small  $\bar{r}$  value due to the incomplete haze removal. Comparatively speaking, our proposed algorithm almost has achieved the best restoration performances in terms of the larger  $\{e, \bar{r}\}$  values and the smaller  $\sigma$  values. For instance, the values of  $\bar{r}$  were larger than 2 when tested on Swans, Pumpkins and Hillside images. That is, our proposed approach was able to preserve more texture details. Remarkably, the values of  $\sigma$  were almost close to zero. Therefore, our proposed approach was able to recover the vivid appearance without sacrificing the color fidelity visually.

#### 4.3. Dehazing and denoising

As discussed in Section 2, most of the current dehazing approaches may not handle the noise problem synchronously. To visually show the noise impact, the salt and pepper noise pattern was first selected for better dehazing illustration. Note that, the salt and pepper noise, sparsely occurring white and black pixels, can be well removed by some pre-processing operations such as

**Table 1**  
Quantitative comparisons with different measurements ( $e$ ,  $\bar{r}$ ,  $\sigma$  and  $\tau$ ).

	He et al. (2011)				Zhu et al. (2015)				Berman et al. (2016)				our			
	$e$	$\bar{r}$	$\sigma$	$\tau$ (s)	$e$	$\bar{r}$	$\sigma$	$\tau$ (s)	$e$	$\bar{r}$	$\sigma$	$\tau$ (s)	$e$	$\bar{r}$	$\sigma$	$\tau$ (s)
Swans	0.411	1.175	0.002	34.437	0.307	1.294	<b>0.000</b>	0.920	<b>0.638</b>	<b>2.933</b>	0.020	1.234	0.597	2.299	0.001	<b>0.726</b>
Pumpkins	0.281	1.619	<b>0.000</b>	34.603	0.168	1.122	<b>0.000</b>	0.979	0.157	1.946	<b>0.000</b>	1.232	<b>0.289</b>	<b>2.217</b>	<b>0.000</b>	<b>0.732</b>
Beijing	0.040	1.454	0.010	34.516	<b>0.123</b>	1.132	<b>0.000</b>	0.945	0.088	1.873	0.110	1.291	0.012	<b>1.881</b>	0.008	<b>0.696</b>
Florence	-0.027	1.411	0.008	116.147	<b>0.033</b>	1.050	<b>0.000</b>	2.827	0.026	1.377	0.008	3.667	0.000	<b>1.987</b>	<b>0.000</b>	<b>1.396</b>
Mountain	<b>0.151</b>	1.180	<b>0.000</b>	29.687	0.102	1.120	<b>0.000</b>	0.816	0.038	1.565	0.013	1.106	0.126	<b>1.573</b>	<b>0.000</b>	<b>0.651</b>
Manhattan	0.045	1.398	<b>0.000</b>	65.864	<b>0.063</b>	1.112	<b>0.000</b>	1.604	-0.056	<b>1.805</b>	0.035	2.236	0.048	1.445	<b>0.000</b>	<b>0.949</b>
Hillside	0.689	2.449	<b>0.000</b>	58.314	0.535	1.488	<b>0.000</b>	1.518	0.526	2.280	<b>0.000</b>	2.065	<b>0.572</b>	<b>2.583</b>	<b>0.000</b>	<b>0.927</b>

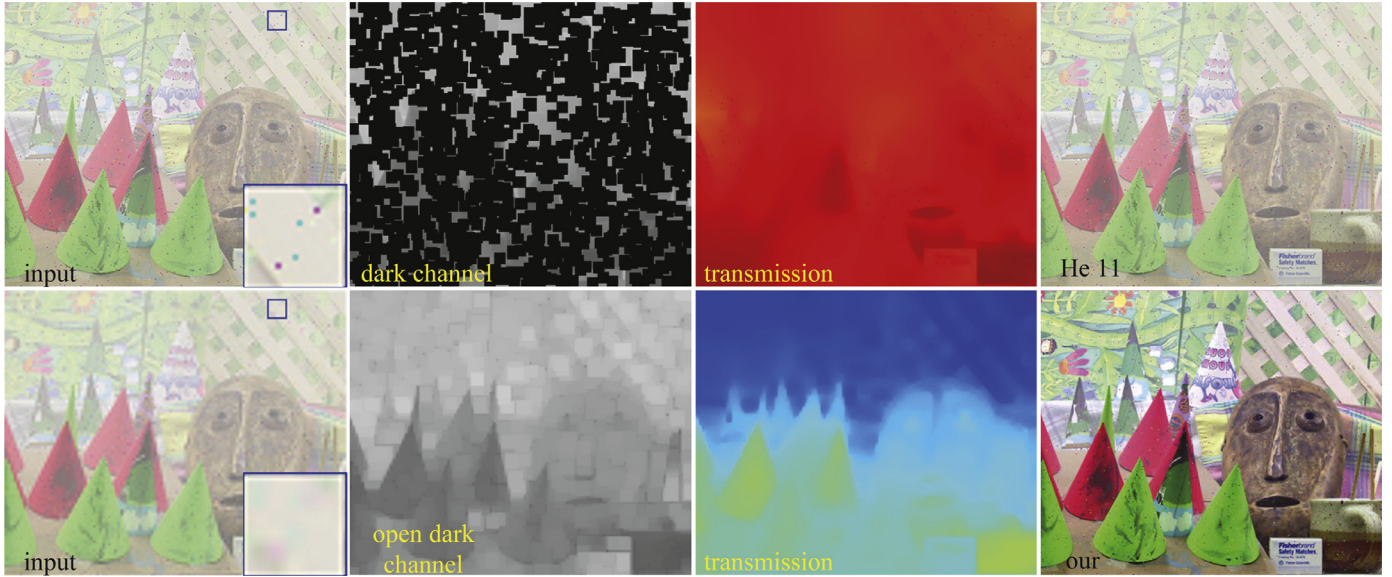


**Fig. 10.** Image dehazing with salt and pepper noise (density = 0.005). From left to right of top row: input image, dark channel, transmission and dehazing results obtained by He et al. (2011). From left to right of bottom row: wavelet decomposition with 'sym4' filter, open dark channel, transmission and dehazing result obtained by the proposed approach.

median filter and morphological filter. As shown in Fig. 10, the DCP method was found to be very sensitive to the apparent noise and the transmission of this prior would be underestimated when there exist obvious noise. The main reason lies that a local patch with significant noise shall make the whole patch darker such that the transmission would be underestimated. Consequently, such underestimated transmission would lead to a dehazing failure. By contrast, our proposed approach is insensitive to the significant noise and the estimated transmission map is accurate enough for efficient haze removal. As a result, the haze impact can be significantly reduced by our proposed approach. The main reasons are two-fold: 1) The salt and pepper noise can be gradually weakened by the wavelet decomposition such that the remaining noise in low frequency shall not significantly affect transmission estimation. 2) Our proposed ODCM method incorporating the morphological open filter is able to well constrain the noise such that transmission can be appropriately estimated for efficient haze removal.

Another representative dehazing and denoising results were shown in Fig. 11, it can be observed that He et al. (2011) has produced a poor dehazing performance when the haze degraded image contains the Gaussian noise. Consequently, the distant regions of the bottom dehazing result were ambiguous. Similarly, Zhu et al. (2015) also failed to remove the haze impact when there existed Gaussian noises and the dehazing result almost shared the similar appearance with the original example. Specifically, Berman et al. (2016) was able to remove the haze to some degree, but which would significantly amplify the noise in remote scenes. Meanwhile, we have selected the professional Adobe Lightroom

2017 software to achieve image dehazing and denoising. By using this software, it can be observed that the significant noise in the distant view cannot be directly removed during the dehazing process. Although the noise can be further reduced by some professional operations, the texture details cannot be well preserved. Fortunately, our proposed approach selected to decompose the hazy image into low frequency part and high frequency parts, whereby the transmission can be well estimated in the low frequency part and the Gaussian noise was almost left in the high frequency parts. Benefit much from wavelet decomposition, the haze can be well removed at the low frequency part, while the texture details were enhanced and Gaussian noise was concurrently reduced in the high frequency parts adaptively. Therefore, as shown in Fig. 11, the proposed approach not only can significantly increase the perceptual visibility of haze scene, but also could preserve more texture details and reduce the noise effect as well. The extensive experiments have shown its outstanding performance.

#### 4.4. Computation time

In the experiments, all the testings were conducted on a desktop computer with an Intel® Core™ i5-3470 GHz processor and 8GB memory, and the coding language was Matlab. Under the same coding condition, we selected to compare the proposed approach with three very competing approaches, i.e., He et al. (2011), Zhu et al. (2015) and Berman et al. (2016). Since the proposed approach employs the wavelet decomposition to reduce the impact of the haze and noise in the degraded scenes, the computational load

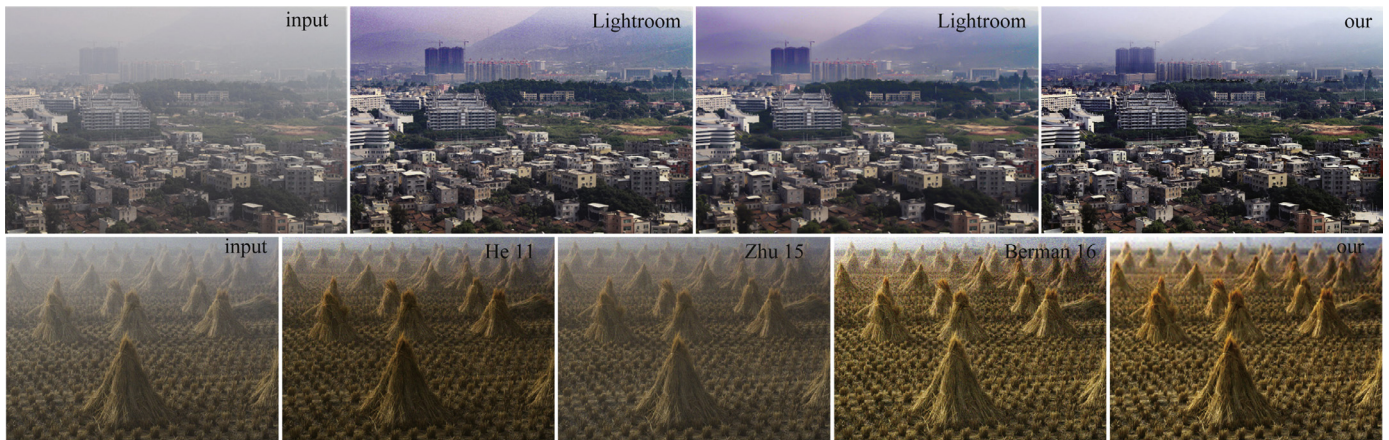


**Fig. 11.** Dehazing and denoising obtained by different approaches. From left to right of top row: input hazy image with heavy haze regions, Adobe Lightroom 2017 dehazing result, Adobe Lightroom 2017 dehazing followed by denoising, our result; From left to right of bottom row: input images with zero-mean Gaussian noise ( $\sigma = 0.02$ ), dehazing obtained He et al. (2011), Zhu et al. (2015), Berman et al. (2016) and our proposed approach, respectively.

would be much more higher than others. Fortunately, the processing time obtained by the proposed approach was really acceptable. As shown in Table 1, the computation times  $\tau$ (s) obtained by the proposed approach were significantly less than the results generated by He et al. (2011), which generally required 30–40 s to process a size of  $600 \times 400$  image. The main reason lies that the soft matting operation in work (He et al., 2011) involves a lot of iterations to refine the transmission map. By contrast, the domain transform filter, favored for its fast implementation, is applied to speed up the dehazing process within our proposed approach.

Further, the computation times obtained by the proposed approach were also less than the results produced by Zhu et al. (2015) and Berman et al. (2016). In essence, these two approaches chose to estimate the transmission maps through the whole image region, and the computation times would grow linearly with the image size by using the guided filtering. In contrast to this, our proposed approach employed the fast wavelet transform to decompose the haze image into several sub-images, and the transmission map was estimated and refined through the low-frequency sub-image, whose scale size was relatively small. For instance, if the decomposition level is 2, the area of low-frequency sub-image is only one-sixteenth of the original image. Accordingly, the main computation time attributed to the transmission map estimation of sub-image would be much smaller than the traditional ways. Although our proposed approach requires an additional decomposition phase, the implementation of fast wavelet transform was very quick and the whole pre-processing time was comparable to these competing approaches. Therefore, the proposed image dehazing and denoising method would be well suitable for recovering the scene contents in real-world images, and experimental results really have shown its outstanding performance.

## 5. Conclusions

In this paper, we have presented an efficient multi-scale correlated wavelet approach for image dehazing and denoising. Under the multi-scale wavelet framework, the haze is typically distributed in the low frequency spectrum. Accordingly, an open dark channel model is presented to achieve low frequency haze removal, and an effective scheme is derived to remove the noise and enhance the texture detail adaptively in the high frequency parts. Consequently, the perceptual visibility of the haze degraded scenes can be significantly increased with visually pleasing texture information and faithful color appearances. Meanwhile, the proposed

approach has demonstrated its efficiency in removing the haze influence and noise impact simultaneously. Benefit much from the wavelet decomposition, our proposed dehazing framework offers a flexible framework to combine with other effective priors or constraints to the scene enhancement. As an efficient image pre-processing method, it is expected that our proposed dehazing and denoising algorithm would be well utilized for various vision degraded applications.

## Acknowledgments

The work described in this paper was supported by the National Science Foundation of China under Grants 61673185, 61672444 and 61772220, the Promotion Program for Young and Middle-aged Teacher in Science and Technology Research of Huaqiao University (No. ZQN-PY309), the National Science Foundation of Fujian Province under Grant 2017J01112, the Science and Technology Research and Development Fund of Shenzhen under Project Code JCYJ20160531194006833, and also partially supported by the Faculty Research Grant of Hong Kong Baptist University (No. FRG2/16-17/051), the Research Grants of University of Macau MYRG2015-00050-FST, and the Macau-China join Project 008-2014-AMJ.

## References

- Ancuti, C.O., Ancuti, C., 2013. Single image dehazing by multi-scale fusion. *IEEE Trans. Image Process.* 22 (8), 3271–3282.
- Berman, D., Treibitz, T., Avidan, S., 2016. Non-local image dehazing. In: Proceedings of the IEEE Conference on Computer Vision and Pattern Recognition, pp. 1674–1682.
- Chen, C., Do, J., Minh, N., Wang, n., 2016. Robust image and video dehazing with visual artifact suppression via gradient residual minimization. In: 14th European Conference on Computer Vision, pp. 576–591.
- Donoho, D.L., 1995. De-noising by soft-thresholding. *IEEE Trans. Inf. Theory* 41 (3), 613–627.
- Du, Y., Guindon, B., Cihlar, J., 2002. Haze detection and removal in high resolution satellite image with wavelet analysis. *IEEE Trans. Geosci. Remote Sens.* 40 (1), 210–217.
- Fattal, R., 2008. Single image dehazing. *ACM Trans. Graph.* 27 (3), 72:1–72:9.
- Fattal, R., 2014. Dehazing using color-lines. *ACM Trans. Graph.* 34 (1), 1–14.
- Gastal, E.S.L., Oliveira, M.M., 2011. Domain transform for edge-aware image and video processing. *ACM Trans. Graph.* 30 (4), 1244–1259.
- Gibson, K.B., Nguyen, T.Q., 2013. Fast single image fog removal using the adaptive Wiener filter. In: Proceedings of the IEEE International Conference on Image Processing, pp. 714–718.
- Gibson, K.B., Vo, D.T., Nguyen, T.Q., 2012. An investigation of dehazing effects on image and video coding. *IEEE Trans. Image Process.* 21 (2), 662–673.
- Hautiere, N., Tarel, J.-P., Aubert, D., Dumont, E., et al., 2008. Blind contrast enhancement assessment by gradient ratioing at visible edges. *Image Anal. Stereol. J.* 27 (2), 87–95.

- He, K., Sun, J., Tang, X., 2009. Single image haze removal using dark channel prior. In: Proceedings of the IEEE International Conference on Computer Vision and Pattern Recognition, pp. 1956–1963.
- He, K., Sun, J., Tang, X., 2011. Single image haze removal using dark channel prior. *IEEE Trans. Pattern Anal. Mach. Intell.* 33 (12), 2341–2353.
- He, K., Sun, J., Tang, X., 2013. Guided image filtering. *IEEE Trans. Pattern Anal. Mach. Intell.* 35 (6), 1397–1409.
- Jobson, D.J., Rahman, Z.U., Woodell, G.A., 1997. A multiscale retinex for bridging the gap between color images and the human observation of scenes. *IEEE Trans. Image Process.* 6 (7), 965–976.
- Katajamäki, J., 2003. Methods for gamma invariant colour image processing. *Image Vis. Comput.* 21 (6), 527–542.
- Kratz, L., Nishino, K., 2009. Factorizing scene albedo and depth from a single foggy image. In: Proceedings of the IEEE International Conference on Computer Vision, pp. 1701–1708.
- Mallat, S.G., 1989. A theory for multiresolution signal decomposition: the wavelet representation. *IEEE Trans. Pattern Anal. Mach. Intell.* 11 (7), 674–693.
- Meng, G., Wang, Y., Duan, J., Xiang, S., Pan, C., 2013. Efficient image dehazing with boundary constraint and contextual regularization. In: Proceedings of the IEEE International Conference on Computer Vision, pp. 617–624.
- Narasimhan, S.G., Nayar, S.K., 2000. Chromatic framework for vision in bad weather. In: Proceedings of the IEEE Conference on Computer Vision and Pattern Recognition, pp. 598–605.
- Narasimhan, S.G., Nayar, S.K., 2003. Contrast restoration of weather degraded images. *IEEE Trans. Pattern Anal. Mach. Intell.* 25 (6), 713–724.
- Rioul, O., Duhamel, P., 1992. Fast algorithms for discrete and continuous wavelet transforms. *IEEE Trans. Inf. Theory* 38 (2), 569–586.
- Rong, Z., Jun, W.L., 2014. Improved wavelet transform algorithm for single image dehazing. *Optik-Int. J. Light Electron Opt.* 125 (13), 3064–3066.
- Schechner, Y.Y., Narasimhan, S.G., Nayar, S.K., 2001. Instant dehazing of images using polarization. In: Proceedings of the IEEE International Conference on Computer Vision and Pattern Recognition, pp. 325–332.
- Tan, R.T., 2008. Visibility in bad weather from a single image. In: Proceedings of the IEEE International Conference on Computer Vision and Pattern Recognition, pp. 1–8.
- Tarel, J.P., Hautiere, N., 2009. Fast visibility restoration from a single color or gray level image. In: Proceedings of the IEEE International Conference on Computer Vision, pp. 2201–2208.
- Xie, B., Guo, F., Cai, Z., 2010. Improved single image dehazing using dark channel prior and multi-scale retinex. In: Proceedings of the IEEE International Conference on Intelligent System Design and Engineering Application, pp. 848–851.
- Xu, H., Zhai, G., Wu, X., Yang, X., 2014. Generalized equalization model for image enhancement. *IEEE Trans. Multimedia* 16 (1), 68–82.
- Zhu, H., Chan, F.H., Lam, F.K., 1999. Image contrast enhancement by constrained local histogram equalization. *Comput. Vis. Image Understand.* 73 (2), 281–290.
- Zhu, Q., Mai, J., Shao, L., 2015. A fast single image haze removal algorithm using color attenuation prior. *IEEE Trans. Image Process.* 24 (11), 3522–3533.